

Stability of spin-driven ferroelectricity in the thin-film limit: Coupling of magnetic and electric order in multiferroic TbMnO₃ films

Artur Glavic,^{1,*} Carsten Becher,² Jörg Voigt,¹ Enrico Schierle,³ Eugen Weschke,³ Manfred Fiebig,² and Thomas Brückel¹

¹Jülich Centre for Neutron Science and Peter Grünberg Institut, JARA-FIT, Forschungszentrum Jülich GmbH, 52425 Jülich, Germany

²Department of Materials, ETH Zurich, Wolfgang-Pauli Strasse 10, CH-8093 Zurich, Switzerland

³Helmholtz-Zentrum Berlin für Materialien und Energie, Elektronenspeicherring BESSY II, Albert-Einstein-Straße 15, 12489 Berlin, Germany

(Received 24 September 2012; revised manuscript received 26 April 2013; published 1 August 2013; publisher error corrected 5 August 2013)

We demonstrate spin-spiral-induced ferroelectricity in epitaxial TbMnO₃ films grown on YAlO₃ substrates down to a film thickness of 6 nm. The ferroelectric polarization is identified by optical second-harmonic generation. Using x-ray resonant magnetic scattering we directly prove the existence of a noncollinear magnetic structure in the ferroelectric phase and thus bulk-like multiferroicity. The electric-field-induced reversal of the magnetic domains along with the reversal of the ferroelectric polarization evidences the rigid coupling of magnetic and ferroelectric order and hence a “giant” magnetoelectric effect in the films.

DOI: [10.1103/PhysRevB.88.054401](https://doi.org/10.1103/PhysRevB.88.054401)

PACS number(s): 42.65.Ky, 61.05.cf, 77.55.Nv, 78.20.Ls

I. INTRODUCTION: THIN-FILM MULTIFERROICS

Competing magnetic interactions in crystals can lead to sinusoidal, helical, or cycloidal spin structures whose periodicity does not follow the periodicity of the lattice. The inherent competition and the low symmetry of such spiral-type structures is a rich source of exotic physical phenomena such as magnetically induced ferroelectricity, complex magnetic excitations such as electromagnons¹ and helimagnons,² or pronounced spin-torque effects.³ There is a great current interest in these phenomena because they throw light on the relation between the spin, charge, and lattice degrees of freedom in systems with multielectron correlations. On the other hand they can also be a basis of future “spintronics” devices such as magnetoresistive or magnetoelectric memories.⁴

The structure of a compound and its functionality is greatly improved by growing it as epitaxial film, possibly even as a constituent in a multilayer heterostructure. In this context, a key question is how robust the spin spirals are against the influence exerted by the substrate and the confinement to a film thickness of only a few spiral periods. There are many examples where the spiral magnetic order is fundamentally altered⁵ or even suppressed,^{6,7} which suggests that the spiral order is in general very sensitive against any form of perturbation and easily destroyed.

A particularly interesting system class expressing this dilemma is compounds with a coexistence of magnetic and magnetically induced ferroelectric order.⁸ These are the so-called spin-spiral multiferroics in which an incommensurate magnetic cycloid or spiral violates inversion symmetry such that a spontaneous polarization becomes allowed. Since the primary order parameter is the magnetic one, the resulting ferroelectricity is called improper.⁹ The best known representative of this group is TbMnO₃. Its multiferroicity was studied extensively and summarized in a complex phase diagram.^{10–12} Consequently, most of the effort to transfer the spin-spiral order of a multiferroic from bulk samples to thin films was devoted to TbMnO₃.^{13–15} These experiments revealed a variety of interesting film properties, among which the most notably may be a magnetization induced by strain.¹³ However, a reproduction of the spiral magnetism has not been achieved so far. The closest approach up to now was the observation

of discontinuities in the magnetic and dielectric response in orthorhombic RMnO₃ films of ≈ 100 nm ($R = \text{Ho, Y, Tm}$),^{16–18} yet without evidence for cycloidal magnetic order. Other experiments on FeVO₄ and Ni₃V₂O₈^{19,20} concentrated on even thicker films, and the magnetic structure was not investigated. A comprehensive review of the different classes of multiferroics and their possible application with a focus on thin films can be found in Ref. 21.

Here we report the presence of a noncollinear spin structure in epitaxial TbMnO₃ thin films and its stability against geometrical confinement. Using x-ray resonant magnetic scattering (XRMS), we directly show that the magnetic spin cycloid coexists and is coupled to a ferroelectric polarization detected by second-harmonic generation (SHG). This multiferroic phase persists at least down to a thickness of 6 nm, corresponding to only 10 monolayers or 3 periods of the spin cycloid. These bulk-like properties with a rigid coupling between the magnetic and electric order are observed for untwinned, single-domain TbMnO₃ films grown nearly strain free on orthorhombic YAlO₃ substrates.²² Manipulation of the magnetic domain structure by an electric field generated via a photoelectric charge or externally proves the giant magnetoelectric response.

II. SAMPLE PREPARATION AND CHARACTERIZATION

We used commercial stoichiometric TbMnO₃ disks to prepare the samples on orthorhombic YAlO₃ (1 0 0) substrates by high-pressure oxygen sputter deposition. At this surface the substrate in-plane lattice (b, c) perfectly fits the TbMnO₃ a and c axes, leading to single-domain films, which was confirmed by x-ray diffraction. Under an oxygen pressure of 3 mbar the material was deposited using a radio-frequency-excited plasma below the target. The substrates had a distance of ≈ 2 cm to the target and were heated to ≈ 700 °C during deposition. X-ray reflectivity and diffraction were used to analyze the quality of the films and measure their thickness. The surface roughnesses range between 0.3 and 1.5 nm. Rocking scans on the (0 2 0) reflection reveal a width of only $\leq 0.05^\circ$ which confirms the excellent epitaxy of the films. The substrate matching is evidenced by reciprocal lattice maps around the (0 2 4) and

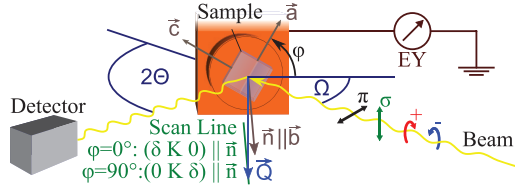


FIG. 1. (Color online) Setup used for the XRMS experiment. The polarization of the incident light is tunable, the scattered intensity is recorded with a diode, and the electron yield current is measured on the copper sample holder. The surface normal \vec{n} always lies in the scattering plane, while the perpendicular direction can be changed manually (angle φ).

(2 2 0) reflections (see Supplemental Material²³). Rutherford backscattering spectrometry verifies that the stoichiometry is correct within the detection limit of 2%.

III. USED EXPERIMENTAL SETUPS

Soft XRMS was performed at the UE46-PGM1 beamline of BESSY II using the XUV diffraction chamber. The setup allows investigations with σ and π linear as well as circular polarized photons at the Mn L and Tb M edges. The samples were mounted on the cryostat cold finger using flat copper cylinders with the surface normal (b direction parallel to the cylinder axis) in the scattering plane (see Fig. 1 and detailed description in Ref. 24).

SHG was performed using 130 fs pulses of 0.954 eV emitted at 1kHz by an optical parametric amplifier. This was pumped by a Ti:sapphire laser system generating amplified pulses at 1kHz and 1.55 eV. The samples were investigated in a transmission setup using a GaAs photomultiplier tube as detector.²⁵

IV. EXPERIMENTAL RESULTS

A. Magnetic order by XRMS

We first investigated the magnetic order of the TbMnO₃ films. As preparation macroscopic magnetization measurements were performed with a Quantum Design SQUID magnetometer, zero-field-cooled, field-cooled, and thermoremanent magnetization measurements with an applied field in the c direction all indicate a phase transition at $T_N \approx 43$ K, i.e., exactly as in the bulk material. This already points to possible bulk-like multiferroicity of the epitaxial films and stimulated a detailed XRMS examination. XRMS allows for the element-specific investigation of magnetic order and has already been applied to bulk RMnO₃ samples.^{26–29} Soft x-ray radiation is capable of studying the magnetization in thin films down to a few monolayers.^{30,31} It provides access to the spatial magnetization components with linearly polarized x rays and to the helicity of magnetic spirals^{28,29} with circularly polarized x rays.

As shown recently,²⁹ the magnetic structure of bulk TbMnO₃ consists of a canted spin density wave below $T_{SDW} \approx 43$ K and a so-called off-phase-synchronized cycloid below $T_C = 27$ K, which induces the ferroelectricity.¹¹ This complicated structure allows two kinds of magnetic satellite reflections (H, $\mathbf{K} \pm \tau_{Mn}$, L): stronger A-type and weaker F-type

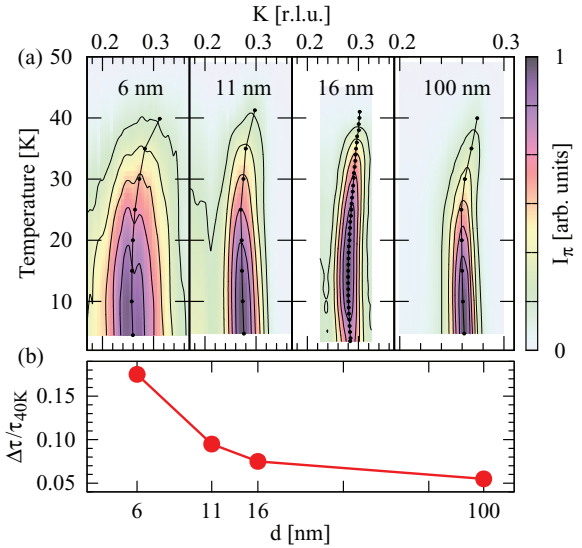


FIG. 2. (Color online) (a) Temperature dependence of the scattering intensity for incident π -polarized radiation at the Mn L₂ edge. The charge-scattering background measured above the ordering temperature has been subtracted from each measurement. Black points indicate the peak center retrieved by a Gaussian fit. (b) Relative shift of the peak-center value of τ_{Mn} between 40 K and its minimum for different values of the film thickness.

reflections with L even and odd, respectively. F-type reflections were investigated by us at the Mn L_{2,3} edge as the long wavelength inhibits access to any other satellite reflection.

Figure 2(a) shows the temperature dependence of the magnetic (0 τ_{Mn} 0) reflection for films of different thickness. For all samples, incommensurate magnetic order is observed with a transition temperature similar to the bulk value. The width of the corresponding peak depends on the film thickness. The Tb propagation vector τ_{Tb} has a value of 0.44 which is very close to the bulk value of 0.43.²⁶ The general trend of τ_{Mn} to decrease from T_{SDW} towards an almost lock-in at T_C is also reported for the bulk but in the films the value of τ_{Mn} shows a larger spread (0.26–0.31 versus 0.275–0.290 in the bulk²⁷). This effect increases for decreasing film thickness as depicted in Fig. 2(b).

Polarization-dependent scattering reveals further details about the magnetic order. In our experimental geometry, the polarization-dependent magnetic XRMS intensities as a function of the scattering angles Ω , 2Θ and site specific saturation magnetization (m_a, m_b, m_c) are given by^{29,32}

$$\varphi = 0^\circ \quad I_\sigma = m_a^2 \cos^2 \Omega + m_b^2 \sin^2 \Omega, \quad (1)$$

$$I_\pi = m_a^2 \cos^2 \Omega + m_b^2 \sin^2 \Omega + m_c^2 \sin^2(2\Theta); \quad (2)$$

$$\varphi = 90^\circ \quad I_\sigma = m_c^2 \cos^2 \Omega + m_b^2 \sin^2 \Omega, \quad (3)$$

$$I_\pi = m_c^2 \cos^2 \Omega + m_b^2 \sin^2 \Omega + m_a^2 \sin^2(2\Theta). \quad (4)$$

At first, the components of the Mn order and their temperature dependence were investigated with linearly polarized x rays. Measurements with φ at 0° and 90° using π and σ incident polarization allow for the determination of the magnetic moment components according to Eqs. (1)–(4). For the spin-density-wave phase, only a c component is present, evidenced by resonant magnetic scattering only for the π

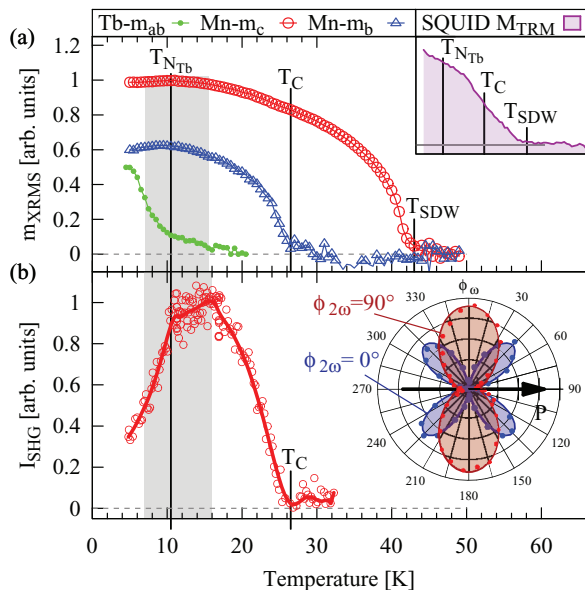


FIG. 3. (Color online) Temperature dependence of the multiferroic order in epitaxial TbMnO₃ films in complementary measurements (a) by XRMS and SQUID magnetometry (inset) and (b) by SHG. (a) The *b* and *c* component of the magnetic Mn order and the *ab* component of the Tb order for a TbMnO₃ film of 11 nm. Data were extracted from intensity measurements of σ - and π -polarized incident light at the (0 τ_{Mn} 0) and (0 τ_{Tb} 0) positions using Eqs. (1)–(4). The curve in the inset shows the thermoremanent magnetization for comparison. (b) SHG intensity from the χ_{caa} component at 1.907 eV for a TbMnO₃ film of 100 nm. The inset shows the polarization anisotropy of the SHG signal at $T = 11$ K. The SHG polarization was fixed at 0° or 90° while rotating the incident-light polarization. Solid lines are fits using Eqs. (5) and (6).

incident beam at $\varphi = 0^\circ$ (Fig. 2). Below T_C additional intensity for σ incident polarization arises, due to a *b* component of the magnetic moments (at $\varphi = 90^\circ$ π and σ intensities are equal, ruling out an *a* contribution). Figure 3(a) shows the temperature dependence of the magnetic order parameters for a film of 11 nm.³³ Below 16 K a gradual emergence (shaded area in Fig. 3) of the Tb order with an inflection point at $T_{N_{\text{Tb}}} \approx 10$ K is observed at (0 τ_{Tb} 0). In contrast the transition occurs abruptly at 7 K in bulk crystals. Along with the change of slope of the spontaneous polarization according to the SHG data in Fig. 3(b), which is not observed in bulk crystals, these differences point to a subtle modification of the Tb-Mn coupling in the films. Note, however, that the Mn propagation vector and transition temperatures are very close to bulk TbMnO₃, even for the thinnest sample with only 6 nm thickness. This shows that TbMnO₃ can be prepared in very thin films without substantial alterations of the magnetic properties.

B. Ferroelectricity by SHG

For probing the ferroelectric order, a TbMnO₃ film was investigated by optical SHG. According to Fig. 2 no qualitative differences exists for films with a thickness between 6 and 100 nm, so that we restricted the optical investigation to the 100-nm film, where the strongest signal is obtained. In the

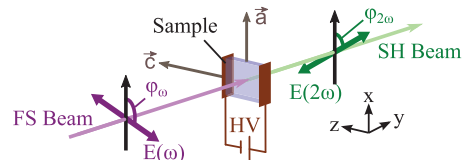


FIG. 4. (Color online) Sketch of the SHG geometry used for the measurements, illustrating the angle of polarization $\varphi_{2\omega, \omega}$ of the SHG and the fundamental light with respect to the sample axes.

leading order, SHG is only allowed in noncentrosymmetric crystals. A spontaneous polarization P_s breaks the inversion symmetry and can therefore be detected background free by the emergence of a SHG signal. This is parametrized by the nonlinear susceptibility components χ_{ijk} with *i* as polarization of the detected frequency-doubled light, and *j* and *k* as polarizations of the incident fundamental light waves. In TbMnO₃, P_s reduces the TbMnO₃ point group symmetry to *mm*2 so that the SHG intensity for light propagating along the *b* axis is given by²⁵

$$I_{\varphi_{2\omega}=0^\circ} \propto |\chi_{aca} \cos(\varphi_\omega) \sin(\varphi_\omega)|^2, \quad (5)$$

$$I_{\varphi_{2\omega}=90^\circ} \propto |\chi_{ccc} \sin^2(\varphi_\omega) + \chi_{caa} \cos^2(\varphi_\omega)|^2. \quad (6)$$

Here, $\varphi_{2\omega}$ and φ_ω denote the polarization of the SHG and the fundamental light, respectively, with respect to the *a* axis.

As depicted in Fig. 4 we irradiated the sample with light at 0.954 eV for which in a SHG spectroscopy measurement (not shown) the maximum SHG signal was obtained. The polarization and temperature dependence of the SHG signal is shown in Fig. 3(b). We clearly observe the emergence of a SHG signal at 27 K, which is exactly the transition temperature into the multiferroic phase in the bulk. In addition the polarization dependence of the SHG signal matches that derived in Eqs. (5) and (6) for a ferroelectric state with spontaneous polarization along the *c* axis. We therefore conclude that aside from the magnetic order, the ferroelectric order of TbMnO₃ is also reproduced in the epitaxial films.

C. Coupled switching of magnetic and electric order

In the next step we scrutinized the coupling between the magnetic and the ferroelectric order as well as the magnetoelectric switching properties of the TbMnO₃ films below $T_C = 27$ K. Note that this is an important missing piece in any investigation of epitaxial films with suspected magnetically induced ferroelectricity so far. The cycloidal magnetic structure $\vec{m}(\vec{r})$ leads to the circular XRMS diffraction intensities I_\pm :^{28,29,34}

$$I_\pm = \frac{I_\pi + I_\sigma}{2} \mp m_b m_c \sin \Omega \sin(2\Theta) \quad (7)$$

$$\text{for } \vec{m}(\vec{r}) = \vec{e}_b m_b \sin(\vec{\tau} \cdot \vec{r}) + \vec{e}_c m_c \cos(\vec{\tau} \cdot \vec{r}). \quad (8)$$

The circular dichroism ($I_+ - I_-$) vanishes for a collinear magnetic structure but also for equal population of left- and right-handed domains. Hence, in order to observe this dichroism, we unbalanced the domain population by charging the samples through the photoelectric effect in the synchrotron beam while cooling them through T_C as described in detail in Ref. 28. As Fig. 5 shows, the charge-induced electric field leads

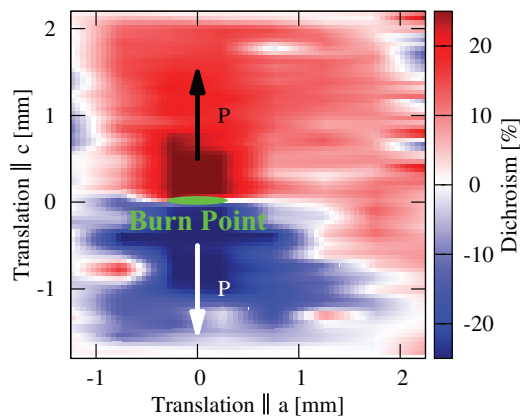


FIG. 5. (Color online) Spatial map of the circular XRMS dichroism measured at $(0 \tau_{\text{Mn}} 0)$ at the Mn L edge of a TbMnO_3 film of 100 nm. The sample was cooled with the x-ray beam at the “burn point” position (green ellipse approximates beam size) and measured at 11 K. The arrows indicate the electric-polarization direction associated with the respective cycloidal domain.

to large regions of different dichroism and, hence, cycloidal handedness above and below the synchrotron burn point. This behavior was reproduced in all our samples down to the thinnest one of 6 nm.

The dichroism vanishes at the multiferroic transition temperature of $T_C \approx 27$ K, while the magnetic scattering is present up to 43 K. Cooling the samples with the beam at different positions shifts the boundary between the oppositely dichroic regions accordingly. This directly proves the control of the sense of rotation of the magnetic cycloid by the electric field exerted by the photoelectrically generated charge at the burn point²³ and, hence, the rigid magnetoelectric coupling in the TbMnO_3 films.

Although the surface map of the XRMS dichroism signal in Fig. 5 reveals two large regions of different magnetic handedness, the contrast between these regions is not uniform which seems to contradict the presence of two discrete magnetic states. We therefore performed additional SHG experiments in an electric field applied directly to the sample via noncontact electrodes and explored the switching behavior of the ferroelectric state. Figure 6 reveals a butterfly loop of the SHG intensity in a field of up to ± 250 V/mm. The butterfly loop reflects the sensitivity of the SHG process to the sign of the spontaneous polarization.²⁵ With the method used in Ref. 35 the SHG signal can thus be converted into the sign-sensitive polarization loop shown as the inset of Fig. 6.

We find a clearly hysteretic behavior. However, the shape of the hysteresis shows that the applied field is not high enough to drive the sample into saturation—the polarization reversal does not engulf the entire sample so that it remains in a multidomain state. SHG imaging experiments reveal a domain size of about $1 \mu\text{m}$. We thus see that the fractional reversal of the polarization domains in Fig. 6 corresponds to a fractional reversal of the magnetic domains in Fig. 5. Higher saturation (and contrast) is observed close to the burn point where the electric field is also higher. This is a striking confirmation of the rigid coupling between the magnetic and ferroelectric order in the films and a demonstration of a giant

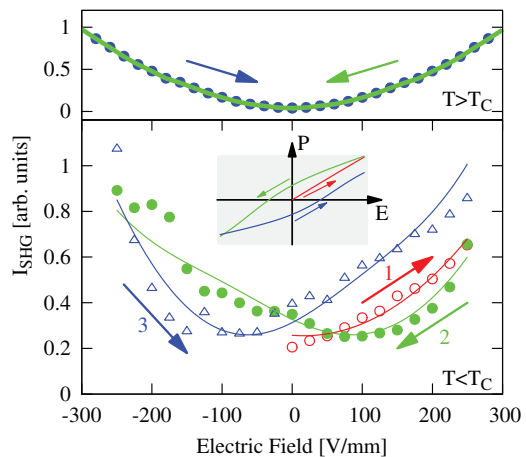


FIG. 6. (Color online) Electric-field dependence of the SHG signal from the 100 nm TbMnO_3 film at 50 K (top) and 15 K (bottom). The field was applied with noncontact electrodes along the c axis. Assuming SHG contributions by the polarization, the electric field, and the crystallographic structure, a polarization hysteresis was fitted to the SHG data according to Ref. 35 (bottom, solid lines). Note that leakiness often produces pseudopolarization loops of a similar shape in pyroelectric current measurements. However, the SHG measurements are not affected by leakiness so that the polarization hysteresis in the inset is genuine.

magnetoelectric effect with electric-field-induced reversal of the magnetic order. Furthermore, this is, to our knowledge, the first time that TbMnO_3 was magnetoelectrically polarized *within* the multiferroic phase.

D. Thin-film vs bulk magnetic order

There are several reasons we can be sure that we observe the same kind of magnetic order as in the bulk case, although we have restricted the investigation of the magnetic order to measuring a single F-type reflection. The transition temperature and the incommensurate propagation vector agree well with the TbMnO_3 bulk value. In Fig. 5 the chirality switches its sign when scanning the sample across the burn point in the c direction. This is only consistent with a polarization directed along the c axis and, thus, with the bulk-type chiral magnetic order. The circular dichroism rules out a collinear arrangement of magnetic moments and its signal strength is orders of magnitude too low for a reflection from a pure F-type order of the Mn magnetic moments.

V. CONCLUSION

In summary, the magnetic spin-spiral structure of bulk TbMnO_3 was successfully transferred to epitaxial films with a thickness of down to only three periods of the cycloidal spiral. Using XRMS and SHG as complementary methods we obtain direct evidence for the presence of a magnetic spiral and a magnetically induced ferroelectric polarization, respectively. The persistence of the multiferroic order in the thin films was achieved by growing the TbMnO_3 nearly strain free on YAIO_3 substrates. The corresponding multiferroic domains have a lateral extension of about $1 \mu\text{m}$. A point charge induced by the photoeffect creates mm-sized magnetic majority domain

regions. In addition, SHG experiments in an electric field show the corresponding reversal of the electric polarization and confirm the rigid coupling of magnetic and ferroelectric order in the TbMnO₃ films. According to these two observations the giant magnetoelectric effect known from the bulk is thus also successfully transferred to the epitaxial films. Our work shows that contrary to previous experience^{6,13} it is possible to sustain magnetic spiral order and the related multiferroicity and giant magnetoelectric coupling even in the presence of pronounced spatial confinement. This opens the possibility to implement

the magnetically induced ferroelectrics as heterostructure constituent and thus further expand their functionality.

ACKNOWLEDGMENTS

We thank Jürgen Schubert and Willi Zander from the Peter Grünbert Institute for the RBS measurement and its evaluation as well as Dennis Meier from ETH Zürich for intensive discussions. Financial support by the SFB 608 of the DFG is appreciated.

*artur.glavic@googlemail.com

¹A. B. Sushkov, R. V. Aguilar, S. Park, S.-W. Cheong, and H. D. Drew, *Phys. Rev. Lett.* **98**, 027202 (2007).

²M. Janoschek, F. Jonietz, P. Link, C. Pfleiderer, and P. Böni, *J. Phys.: Conf. Ser.* **200**, 032026 (2010).

³I. N. Krivorotov, N. C. Emley, J. C. Sankey, S. I. Kiselev, D. C. Ralph, and R. A. Buhrman, *Science* **307**, 228 (2005).

⁴M. Bibes and A. Barthelemy, *Nat. Mater.* **7**, 425 (2008).

⁵S. X. Huang and C. L. Chien, *Phys. Rev. Lett.* **108**, 267201 (2012).

⁶T. Zhao, A. Scholl, F. Zavaliche, K. Lee, M. Barry, A. Doran, M. P. Cruz, Y. H. Chu, C. Ederer *et al.*, *Nat. Mater.* **5**, 823 (2006).

⁷R. Ramesh and N. A. Spaldin, *Nat. Mater.* **6**, 21 (2007).

⁸S.-W. Cheong and M. Mostovoy, *Nat. Mater.* **6**, 13 (2007).

⁹V. K. Wadhawan, *Introduction to Ferroic Materials* (Gordon and Breach Science Publishers, Tokyo, 2000).

¹⁰T. Kimura, T. Goto, H. Shintani, K. Ishizaka, T. Arima, and Y. Tokura, *Nature (London)* **426**, 55 (2003).

¹¹M. Kenzelmann, A. B. Harris, S. Jonas, C. Broholm, J. Schefer, S. B. Kim, C. L. Zhang, S. W. Cheong, O. P. Vajk, and J. W. Lynn, *Phys. Rev. Lett.* **95**, 087206 (2005).

¹²M. Mostovoy, *Phys. Rev. Lett.* **96**, 067601 (2006).

¹³B. J. Kirby, D. Kan, A. Luykx, M. Murakami, D. Kundaliya, and I. Takeuchi, *J. Appl. Phys.* **105**, 7D917 (2009).

¹⁴D. Rubi, C. de Graaf, C. J. M. Daumont, D. Mannix, R. Broer, and B. Noheda, *Phys. Rev. B* **79**, 014416 (2009).

¹⁵X. Marti, V. Skumryev, C. Ferrater, M. V. Garcia-Cuenca, M. Varela, F. Sanchez, and J. Fontcuberta, *Appl. Phys. Lett.* **96**, 222505 (2010).

¹⁶T. C. Han and J. G. Lin, *Appl. Phys. Lett.* **94**, 082502 (2009).

¹⁷I. Fina, L. Fabrega, X. Marti, F. Sanchez, and J. Fontcuberta, *Phys. Rev. Lett.* **107**, 257601 (2011).

¹⁸T. C. Han and H. H. Chao, *Appl. Phys. Lett.* **97**, 232902 (2010).

¹⁹A. Dixit, G. Lawes, and A. B. Harris, *Phys. Rev. B* **82**, 024430 (2010).

²⁰C. Sudakar, P. Kharel, R. Naik, and G. Lawes, *Phil. Mag. Lett.* **87**, 223 (2007).

²¹G. Lawes and G. Srinivasan, *J. Phys. D: Appl. Phys.* **44**, 243001 (2011).

²²A. Glavic, J. Voigt, J. Persson, Y. X. Su, J. Schubert, J. de Groot, W. Zande, and T. Brückel, *J. Alloys Compd.* **509**, 5061 (2011).

²³Additional experimental results can be found in the Supplemental Material at <http://link.aps.org/supplemental/10.1103/PhysRevB.88.054401>.

²⁴J. Fink, E. Schierle, E. Weschke, and J. Geck, *Rep. Prog. Phys.* **76**, 056502 (2013).

²⁵M. Fiebig, V. V. Pavlov, and R. V. Pisarev, *J. Opt. Soc. Am. B* **22**, 96 (2005).

²⁶J. Stremper, B. Bohnenbuck, I. Zegkinoglou, N. Aliouane, S. Landsgesell, M. v. Zimmermann, and D. N. Argyriou, *Phys. Rev. B* **78**, 024429 (2008).

²⁷J. Voigt, J. Persson, J. W. Kim, G. Bihlmayer, and T. Brückel, *Phys. Rev. B* **76**, 104431 (2007).

²⁸E. Schierle, V. Soltwisch, D. Schmitz, R. Feyerherm, A. Maljuk, F. Yokaichiya, D. N. Argyriou, and E. Weschke, *Phys. Rev. Lett.* **105**, 167207 (2010).

²⁹H. Jang, J.-S. Lee, K.-T. Ko, W.-S. Noh, T. Y. Koo, J.-Y. Kim, K.-B. Lee, J.-H. Park, C. L. Zhang *et al.*, *Phys. Rev. Lett.* **106**, 047203 (2011).

³⁰C. Schüßler-Langeheine, J. Schlappa, A. Tanaka, Z. Hu, C. F. Chang, E. Schierle, M. Benomar, H. Ott, E. Weschke, G. Kaindl, O. Friedt, G. A. Sawatzky, H.-J. Lin, C. T. Chen, M. Braden, and L. H. Tjeng, *Phys. Rev. Lett.* **95**, 156402 (2005).

³¹E. Weschke, H. Ott, E. Schierle, C. Schüßler-Langeheine, D. V. Vyalikh, G. Kaindl, V. Leiner, M. Ay, T. Schmitte *et al.*, *Phys. Rev. Lett.* **93**, 157204 (2004).

³²S. W. Lovesey and S. P. Collins, *X-Ray Scattering and Absorption by Magnetic Materials* (Oxford University Press, New York, 1996).

³³The temperature dependence of the peak position is small compared to the peak width.

³⁴J. C. Lang, D. R. Lee, D. Haskel, and G. Srajer, *J. Appl. Phys.* **95**, 6537 (2004).

³⁵D. Meier, M. Maringer, Th. Lottermoser, P. Becker, L. Bohatý, and M. Fiebig, *Phys. Rev. Lett.* **102**, 107202 (2009).